NASA Technical Memorandum 102809

Flight Data Acquisition Methodology for Validation of Passive Ranging Algorithms for Obstacle Avoidance

Phillip N. Smith

October 1990

National Aeronautics and Space Administration

NASA Technical Memorandum 102809

Flight Data Acquisition Methodology for Validation of Passive Ranging Algorithms for Obstacle Avoidance

Phillip N. Smith
Ames Research Center, Moffett Field, California

October 1990

National Aeronautics and
Space Administration

Ames Research Center
Moffett Field, California 94035-1000

SUMMARY

The automation of low-altitude rotorcraft flight depends on the ability to detect, locate, and navigate around obstacles lying in the rotorcraft's intended flightpath. Computer vision techniques provide a passive method of obstacle detection and range estimation, for obstacle avoidance. Several algorithms based on computer vision methods have been developed for this purpose using laboratory data; however, further development and validation of candidate algorithms require data collected from rotorcraft flight. A data base containing low-altitude imagery augmented with the rotorcraft and sensor parameters required for passive range estimation is not readily available. This paper focuses on the methodology used to develop such a data base from flight-test data consisting of imagery, rotorcraft and sensor parameters, and ground-truth range measurements. As part of the data preparation, a technique for obtaining the sensor calibration parameters is described. The data base will enable the further development of algorithms for computer vision–based obstacle detection and passive range estimation, as well as provide a benchmark for verification of range estimates against ground-truth measurements.

INTRODUCTION

To minimize the risk of detection in high-threat environments, rotorcraft fly at low altitudes so the pilots can use natural terrain, vegetation, and manmade structures to mask the rotorcraft's presence. As the rotorcraft approaches the terrain, the degree of concealment increases; however, pilot workload also increases because the same objects that provide concealment constitute an obstacle course that must be negotiated by the pilot. Figure 1 depicts three modes of low-altitude rotorcraft flight. The most effective and complex of these is nap-of-the-Earth (NOE) flight, during which the rotorcraft executes both lateral and vertical maneuvers below treetop level. The obstacle avoidance task during NOE flight is demanding, leaving the pilot little opportunity to focus on mission-related activities. Mission effectiveness can be increased by developing automation tools to assist the pilot in obstacle avoidance, thus enabling greater attention to be focused on meeting the mission objectives (ref. 1).

The automation tools must be able to perform obstacle detection and range estimation in order to collect information about the surrounding environment. Operationally, these requirements will likely be met through a combination of active sensors, such as millimeter-wavelength radar or laser range scanners, and passive sensors, such as forward-looking infrared (FLIR) imaging systems or low-light-level television (LLLTV) cameras. Reliance on passive sensors whenever feasible, however, will minimize the risk of detection, so it is of interest to determine the degree to which obstacle detection requirements can be met solely through the use of passive sensors. If the detection requirements cannot be met using passive sensors alone, supplementary data can be acquired by the minimal use of active sensors directed selectively, based on the passive sensor information.

NASA, in cooperation with the U.S. Army, has initiated a program to determine the extent to which passive range estimation can be used as a basis for obstacle avoidance. Several methods have been developed to perform passive range estimation (refs. 2-6), and early algorithms have been tested on laboratory data with promising results. Further development of passive range estimation algorithms for use in obstacle avoidance during NOE flight requires data collected through actual rotorcraft flight, including not only the measurements required to perform passive range estimation but also measurements of true range for

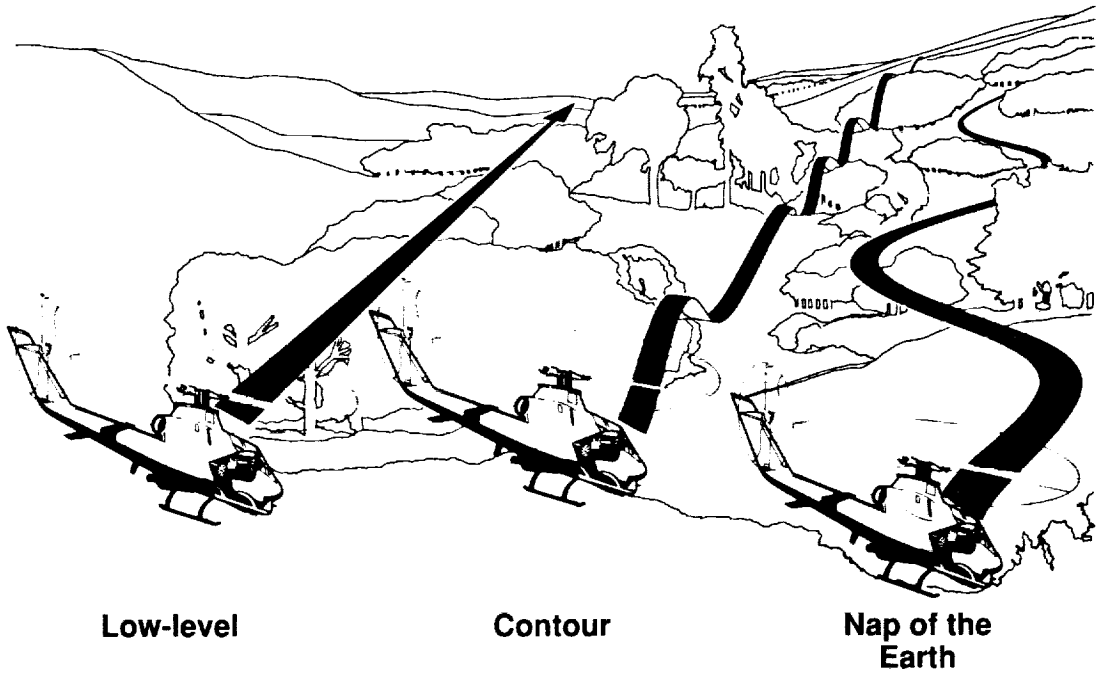

Figure 1. Three modes of low-altitude rotorcraft flight.

validation. The purposes of this paper are to present a methodology used to develop the required data set and to describe the resulting data set.

One method of obstacle detection and range estimation is based on computer vision techniques that operate on a sequence of images. This paper focuses on the analysis of video-type imagery, but the same techniques also apply to other types of imagery, such as FLIR, which could lead to a nighttime-capable system. These techniques are based on the well-defined relationships among the sensor motion, the apparent motion over time of obstacles in the sensor imagery, and the position of the obstacles relative to the sensor. We assume that sensor motion is known through measurements made by an inertial navigation system onboard the rotorcraft; we are interested only in determining the locations of obstacles.

This paper first provides a general description of the passive ranging concept, for the purpose of defining the data requirements. Descriptions follow of the flight experiment, the procedures used in processing the flight data, and the experimental method developed to determine the characteristic parameters of the sensor. A general discussion of the resulting data set and plans for future activities completes the paper.

The author wishes to acknowledge his colleague Ray Suorsa for his valuable assistance and suggestions throughout flight test and sensor calibration.

PASSIVE RANGING CONCEPTS

Consider a rotorcraft-mounted sensor that is in motion with respect to an inertial, Earth-fixed frame of reference while it observes an obstacle P whose location is fixed in the Earth frame, as shown in figure 2.

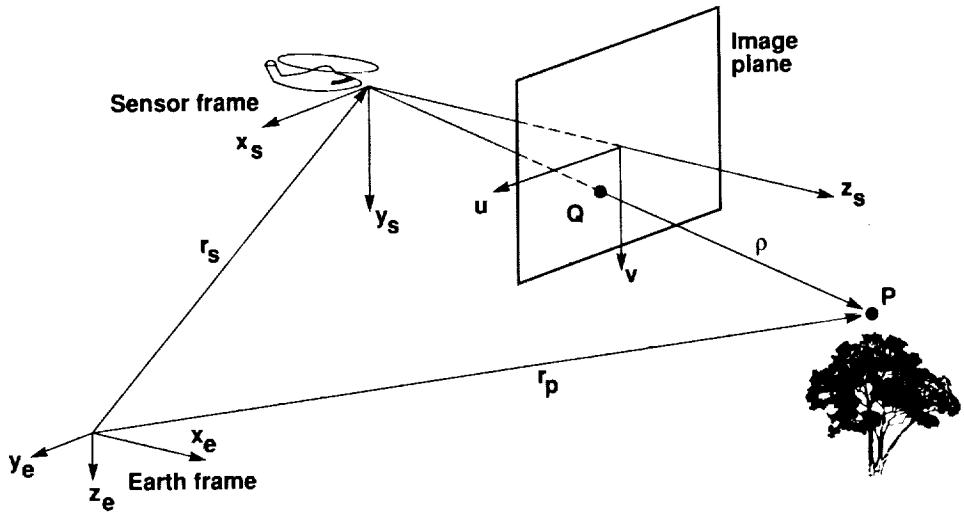

Figure 2. Passive ranging geometry.

We wish to determine the relative position of the obstacle P with respect to the sensor,

$$\rho = r_p - r_s \tag{1}$$

The imaging sensor maps the obstacle P, whose location in sensor coordinates is $\rho_s \triangleq [\rho_{x_s}, \rho_{y_s}, \rho_{z_s}]^T$, onto the image plane at Q by perspective projection, as follows:

$$\begin{bmatrix} u \\ v \end{bmatrix} = \begin{bmatrix} f\rho_{x_s}/\rho_{z_s} \\ f\rho_{y_s}/\rho_{z_s} \end{bmatrix} \tag{2}$$

where f is the focal length, a characteristic of the sensor.

As the sensor moves, ρ_s changes, so the location of the image point Q changes according to

$$\begin{bmatrix} \dot{u} \\ \dot{v} \end{bmatrix} = \frac{1}{\rho_{z_s}} \begin{bmatrix} f\dot{\rho}_{x_s} - u\dot{\rho}_{z_s} \\ f\dot{\rho}_{y_s} - v\dot{\rho}_{z_s} \end{bmatrix} \tag{3}$$

Because the sensor frame is moving, the derivative of ρ_s is determined using the Coriolis equation

$$\dot{\rho}_e = \dot{\rho}_s + \omega \times \rho \tag{4}$$

where $\dot{\rho}_e$ is the derivative of ρ in the Earth frame and is equal to the negative of the sensor velocity in the Earth frame, $\dot{\rho}_s$ is the derivative of ρ in the sensor frame, and ω is the rotation of the sensor frame relative to the Earth frame. Let $V_s \triangleq [V_{x_s}, V_{y_s}, V_{z_s}]^T$ and $\omega_s \triangleq [\omega_{x_s}, \omega_{y_s}, \omega_{z_s}]^T$ be the linear and angular velocities of the sensor with respect to the Earth frame and resolved into sensor coordinates. Then, noting that P is fixed in the Earth frame, we use equations (1) and (4) to obtain

$$\dot{\rho}_s = -V_s - \omega_s \times \rho_s \tag{5}$$

The motion of the image point Q can now be written in terms of the sensor motion using equations (3) and (5):

$$\dot{u} = \dot{u}_T + \dot{u}_R \tag{6a}$$

$$\dot{v} = \dot{v}_T + \dot{v}_R \tag{6b}$$

where the image-point motion has been separated into components resulting from the translational and rotational motion of the sensor, denoted by the subscripts T and R. The components are defined as

$$\dot{u}_T = (-fV_{x_s} + uV_{z_s})/\rho_{z_s} \tag{6c}$$

$$\dot{v}_T = (-fV_{y_s} + vV_{z_s})/\rho_{z_s} \tag{6d}$$

$$\dot{u}_R = \frac{uv}{f}\omega_{x_s} - f\left(1 + \frac{u^2}{f^2}\right)\omega_{y_s} + v\omega_{z_s} \tag{6e}$$

$$\dot{v}_R = f\left(1 + \frac{v^2}{f^2}\right)\omega_{x_s} - \frac{uv}{f}\omega_{y_s} + u\omega_{z_s} \tag{6f}$$

This motion of the image point Q caused by sensor motion is known as optical flow. It is assumed that V_s and ω_s can be derived from the rotorcraft's inertial navigation system; this will be addressed in the next section. If the sensor motion, the focal length, and the optical flow are known, the range, ρ_{z_s}, of the object P corresponding to the image point Q can be determined from the optical flow equations (eqs. (6)). The full vector ρ_s can then be recovered by using the perspective projection equation (eq. (2)).

DATA REQUIREMENTS

In order to test passive range estimation algorithms, it is necessary to have measurements of the sensor motion, V_s and ω_s; knowledge of the focal length, f; and a sequence of images in which the location of any image point can be determined in $[u, v]$ coordinates. The optical flow information $[\dot{u}, \dot{v}]$ is extracted from the image sequence by tracking over time the location of the image point Q corresponding to an obstacle P. This completes the set of data required to perform passive range estimation. Measurements of the actual range are also necessary for comparison with the results of the ranging algorithms.

The sensor motion can be determined from the rotorcraft's velocity, V_b, and angular rates, ω_b, both measured in the rotorcraft body frame of reference. Using the Coriolis equation and the well known coordinate transformation equations, we have

$$V_s = T_{bs}(V_b + \omega_b \times \rho_{bs})$$

$$\omega_s = T_{bs}\omega_b \tag{7}$$

where ρ_{bs} is the vector extending from the body origin to the sensor origin and T_{bs} is the direction cosine matrix, defined by three Euler angles (see table 1), that specifies the orientation of the sensor frame relative to the body frame. The three-element position vector ρ_{bs} and the three Euler angles that define T_{bs} are known as the external camera parameters.

Table 1. Definition of direction cosine matrix

$$T_{bs}(\psi,\theta,\phi) = \begin{bmatrix} 0 & 1 & 0 \\ 0 & 0 & 1 \\ 1 & 0 & 0 \end{bmatrix} \begin{bmatrix} T_{11} & T_{12} & T_{13} \\ T_{21} & T_{22} & T_{23} \\ T_{31} & T_{32} & T_{33} \end{bmatrix}$$

$$\begin{aligned} T_{11} &= c\psi c\theta & T_{12} &= s\psi c\theta \\ T_{13} &= -s\theta & T_{21} &= c\psi s\theta s\phi - s\psi c\phi \\ T_{22} &= s\psi s\theta s\phi + c\psi c\phi & T_{23} &= c\theta s\phi \\ T_{31} &= c\psi s\theta c\phi + s\psi s\phi & T_{32} &= s\psi s\theta c\phi - c\psi s\phi \\ T_{33} &= c\theta c\phi \end{aligned}$$

Note that the sensor frame described by ρ_{bs} and T_{bs} is not defined by any external physical features of the camera, but reflects the location of the focal point and the orientation of the image plane, as illustrated in figure 3. The image plane is formed by a 1/4-inch-square, electronic charge-coupled device (CCD) array located inside the camera. The x_s and y_s sensor axes are parallel to the image-plane axes $[u, v]$ and are oriented along the rows and columns of the CCD array. The z_s axis lies along the principal ray and is orthogonal to the image plane. The origin of the sensor frame is located at the camera focal point.

The location of an image point in $[u, v]$ coordinates can be determined from the digitized images according to the relationships

$$\begin{aligned} u &= (n_u - n_{u0})\ \delta u/\alpha \\ v &= (n_v - n_{v0})\ \delta v \end{aligned} \tag{8}$$

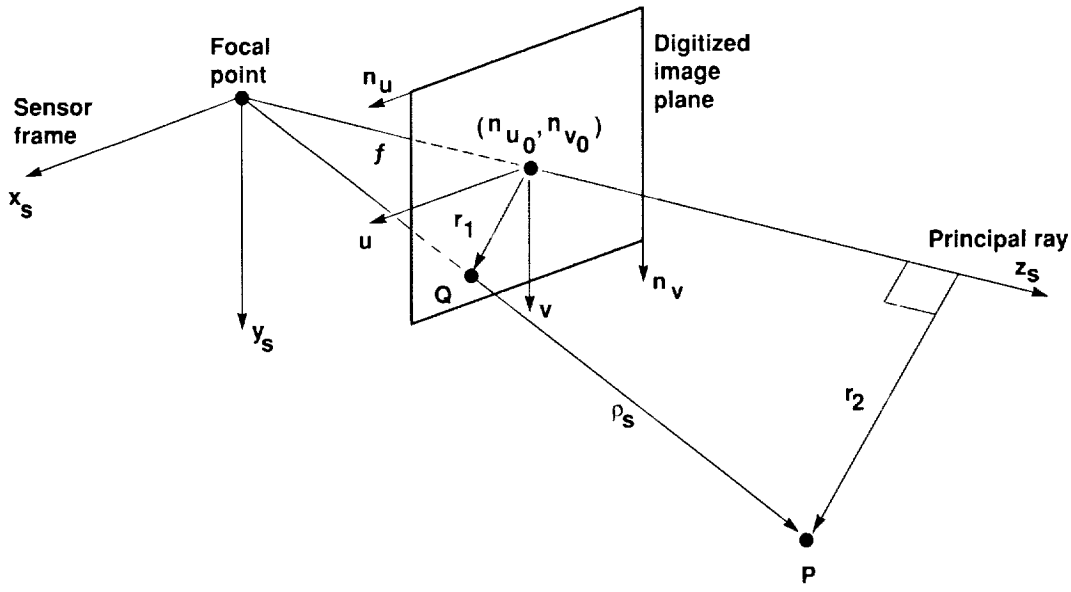

Figure 3. Sensor model.

where $[n_u, n_v]$ are the measured row-column indices of a picture element (pixel) in the digitized image array; $[n_{u_0}, n_{v_0}]$ are the row-column indices of the piercing point, where the principal ray intersects the digitized image plane; $[\delta u, \delta v]$ are the physical spacing of the CCD array elements (available from the camera manufacturer); and α is a scaling parameter, introduced by the digitization process, that defines the mapping between the CCD array elements in the camera and the pixels in the digitized image array. The four parameters n_{u_0}, n_{v_0}, α, and f, the focal length, are known as the internal camera parameters.

To understand the need for the scaling parameter, α, it is necessary to understand the method used to digitize an image generated by the CCD array sensor. Once the CCD array has been exposed, the intensity values registered by the array elements are read out row by row, producing a video signal in the form of an analog voltage waveform. This analog video signal must be digitized so the image can be processed by a computer. A timing mark in the video signal at the beginning of each new row ensures the preservation of the vertical dimension of the image during digitization; however, if the digitization sampling rate differs from the rate at which the CCD array elements of a row are read out to form the video signal, then the horizontal dimension corresponding to a digitized pixel will differ from that of a CCD array element by a scale factor α. For a typical 512×512 pixel image, a small discrepancy in sampling rate can lead to a significant error in the u-coordinate of a feature located near the edge of the image.

Figure 4 summarizes the data and analysis required to validate passive range estimation algorithms. The data set comprises digitized imagery data in the $[n_u, n_v]$ coordinate system, the results of an extensive camera calibration to provide the six external and four internal camera parameters, rotorcraft motion state data, and measurements of actual rotorcraft position relative to the obstacles. The development of the data set is considered in two sections. First is the acquisition of the flight data, including imagery data, rotorcraft state measurements, and radar tracking data for true range information, all of which must be time correlated. Second is the calibration of the imaging sensor, in this case a video camera.

FLIGHT DATA COLLECTION

The flight experiment designed to collect the necessary data is depicted in figure 5. The sensor platform was a CH-47B Chinook helicopter, onboard which a video collection and recording system was installed for the acquisition of the imagery data. A Cohu 6400-series video camera was rigidly mounted under the rotorcraft nose and oriented roughly along the direction of flight so as to observe designated obstacles that the rotorcraft would encounter. The camera's position and orientation with respect to the rotorcraft was held constant throughout the flight project.

To determine the rotorcraft motion states, the following measurements were acquired by instrumentation (listed in parentheses) onboard the CH-47 and telemetered to the ground station at the test-flight facility for recording: (1) longitudinal and lateral inertial velocities (Doppler radar), (2) linear accelerations (accelerometers), (3) Euler angles (inertial navigation system), and (4) angular rates (rate gyros).

To ensure that the derived rotorcraft velocities and rotational rates were as accurate as possible, these data were processed using state estimation algorithm referred to as SMACK (Bach, R. E., Jr.: State Estimation Applications in Aircraft Flight-Data Analysis (A User's Manual for SMACK), to be published as NASA Ames Reference Publication). This algorithm uses the well-known set of rigid-body dynamical equations of motion as a model, processing the measurements together in an "optimal" way to ensure

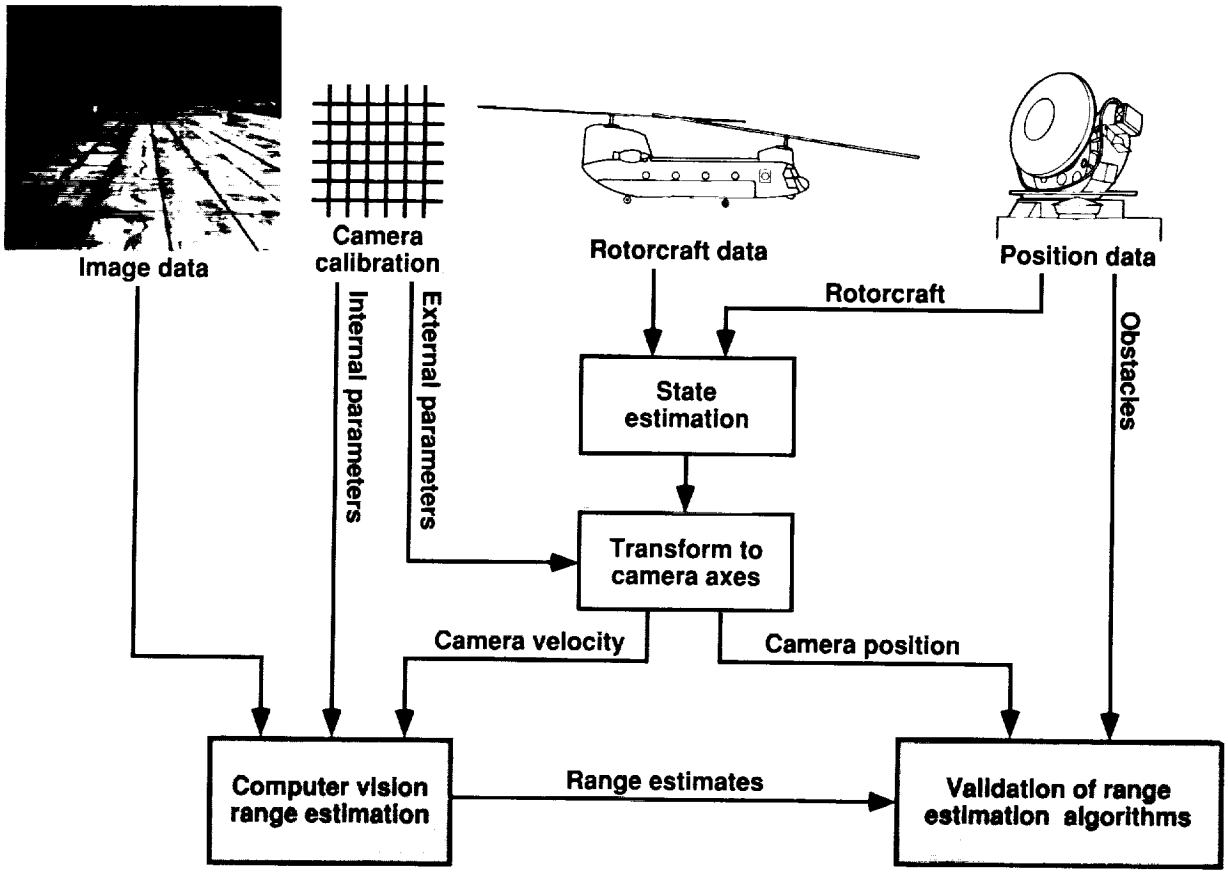

Figure 4. Major elements of the data set.

the internal consistency of measured states, improve the knowledge of poorly measured or unmeasured states, identify instrument-bias errors and scale-factor errors, and estimate the states during brief periods of telemetry dropout. In this way, a best estimate of the rotorcraft's position, orientation, velocity, and angular rates was obtained, based on all available measurements. It is important to note that state estimation is used to develop a high-precision, internally consistent data set for research purposes. An operational sytstem for passive range estimation would acquire rotorcraft state information directly from onboard sensors.

True range measurements were obtained by a two-step process using a laser tracker. First, the laser tracker measured the position of the rotorcraft throughout each test flight. The resulting data was recorded at the ground station on a common time base with the telemetry data. Second, at the completion of a test flight, the laser was used to measure the position of the (stationary) objects that served as the designated obstacles.

To reference the imagery data with the rotorcraft state data and the true range measurements, a time source onboard the CH-47 was synchronized with the time source at the ground station to 1-msec accuracy. Subsequently, a message containing the current time was overlaid on the upper left-hand corner of each video image.

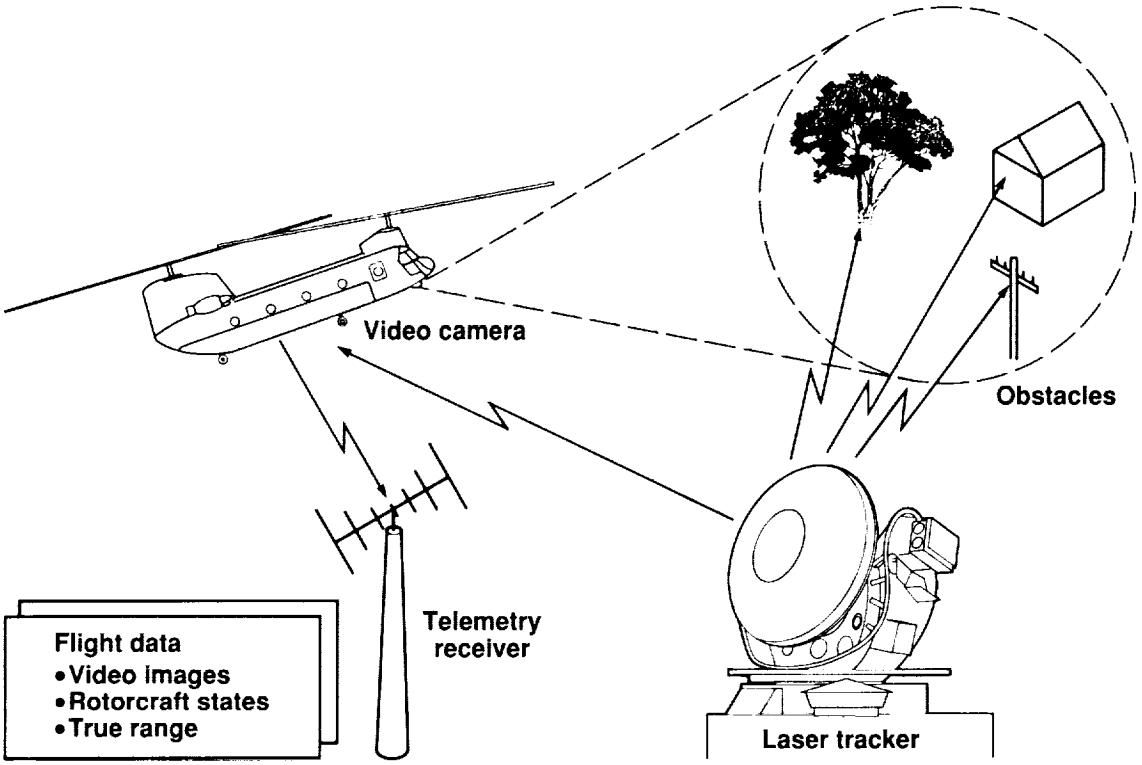

Figure 5. Flight experiment overview.

To simulate typical NOE maneuvers, test flights were conducted within about 40 ft of the ground at speeds not exceeding 40 knots. Typical flight profiles were straight-and-level flight, banked-and-curved flight, pedal turns, bob-ups, and transitions to and from hover. In addition, obstacles were chosen to represent varying levels of difficulty of detection; land vehicles, buildings, transmission towers, natural terrain, and vegetation were used.

CAMERA CALIBRATION

It is difficult to directly measure the values of any camera parameters to a sufficiently high degree of accuracy, so the values of the 10 unknown parameters must be determined experimentally. This is possible because the external parameters (ρ_{bs} and T_{bs}) define how the location of a point P known in body coordinates, ρ_b, is transformed into sensor coordinates,

$$\rho_s = T_{bs}(\rho_b - \rho_{bs}) \tag{9}$$

and the internal parameters (n_{u_0}, n_{v_0}, α, and f) define how the point is subsequently mapped from the sensor frame to some measurable pixel location in a digitized image produced by the sensor,

$$\begin{aligned} n_u &= n_{u_0} + \alpha f\,(\rho_{x_s}/\rho_{z_s})\,/\delta u \\ n_v &= n_{v_0} + f\,(\rho_{y_s}/\rho_{z_s})\,/\delta v \end{aligned} \tag{10}$$

Thus, measurement of object locations in the body frame and measurement of the corresponding pixel locations in the digitized image provide the necessary data for determining the unknown parameters. Note

that the data should exhibit variation in ρ_{z_s} in order to permit robust separation of the focal length, f, from the component of ρ_{bs} along the principal ray during parameter estimation. Substitution of equation (9) into equation (10) yields 2 nonlinear equations in the 10 unknown parameters, so a minimum of 5 measurements of ρ_b and $[\, n_u, n_v \,]$ are required to uniquely determine the parameter values; however, because the emphasis here is on accuracy, it is desirable to have redundant measurements and to use a least squares method to solve the equations.

To acquire the necessary data, a calibration grid was constructed to provide known calibration points P that would represent obstacles. Figure 6 shows the experimental setup for collecting the calibration data. The rotorcraft was placed at an arbitrary location on the ground with the calibration grid positioned in the sensor field of view. The calibration points were the intersections of the horizontal and vertical grid lines. The first objective was to measure the location of the calibration points with respect to the rotorcraft body axes, but the position and orientation of the body frame were unknown. The rotorcraft manufacturer provided the locations in body coordinates of distinctive, accurately known, external rotorcraft features. An arbitrary, user-defined coordinate system was then established at the location of a transit and laser distance-measuring equipment (DME); this allowed range, bearing, and elevation measurements to be made of the external rotorcraft features. Solution of an over-determined triangulation problem yielded the location and orientation of the body frame relative to the user frame. The same transit and laser distance-measuring equipment were then used to measure the locations of the calibration points on the calibration grid with respect to the user axes. Finally, knowing the locations of the calibration points in user coordinates and the relationship between user and body frames, the positions of the calibration points in body coordinates were determined. This procedure was repeated with two different user coordinate systems to improve accuracy and confidence in the results.

The pixel location corresponding to each calibration point was determined manually from the image generated by the sensor. To measure the pixel locations of the calibration points to sub-pixel accuracy, a calibration grid arrangement, rather than isolated calibration points, was used, in the following manner. The image intensity profile perpendicular to a grid line was viewed and the peak of the profile interpolated to obtain, to sub-pixel accuracy, a point on the center of the line. A series of these points were then used to

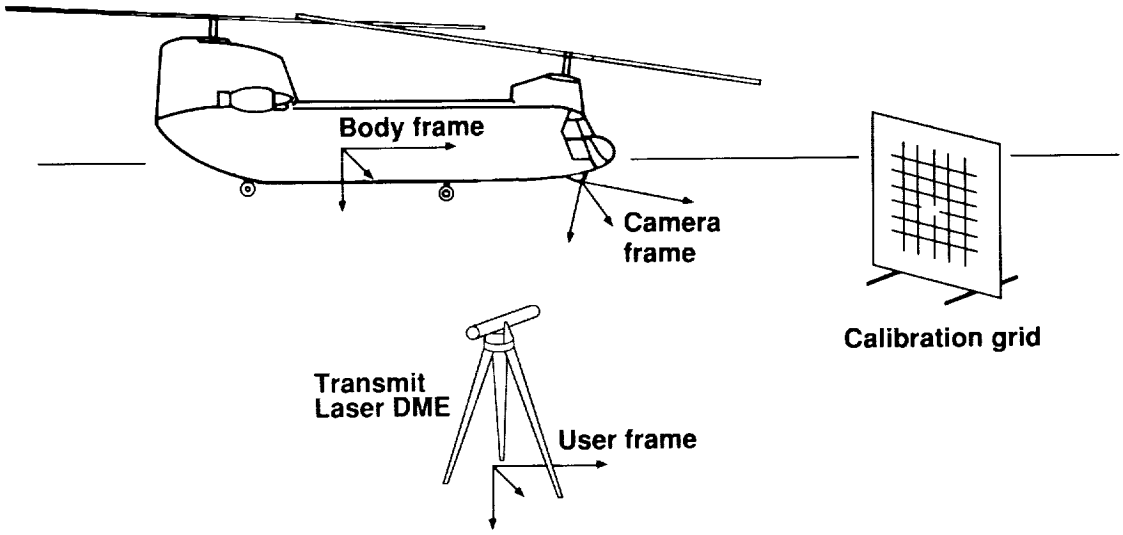

Figure 6. Data collection setup for camera calibration.

reconstruct the true line using a least-squares line-fitting algorithm. The intersection of two lines identified in this manner determined the location of a calibration point to sub-pixel accuracy. The entire calibration process was repeated with the calibration grid in a different location to ensure sufficient variation in ρ_{z_s}.

A method was developed that uses a Newton-Raphson technique to solve the nonlinear least-squares problem to determine the unknown parameters. The method is based on the work of Tsai (ref. 7) but has additional provisions to allow estimation of the piercing point location, $[n_{u_0}, n_{v_0}]$. The cost function to be minimized contains penalty terms for the discrepancy between the measured and predicted image plane location $[n_u, n_v]$ of each calibration point and for violation of the radial alignment constraint (RAC). The RAC states that the vector r_1 from the piercing point to an image point Q must be parallel to r_2, the vector component of ρ_s parallel to the image plane (see fig. 3). A more detailed discussion of the parameter estimation technique is beyond the scope of this paper; however, the parameter estimates obtained are given in table 2.

Table 2. Camera calibration parameters

Parameter	Estimated value[a]	Uncertainty of estimate	Units
ρ_{bs_x}	275.4	0.5	in.
ρ_{bs_y}	–12.5	0.2	in.
ρ_{bs_z}	83.3	0.2	in.
ψ_{bs}	0.3	0.2	deg
θ_{bs}	–8.0	0.2	deg
ϕ_{bs}	–0.4	0.1	deg
n_{u_0}	253.3	2.4	pixels
n_{v_0}	238.3	1.6	pixels
α	1.005	0.001	none
f	0.242	0.001	in.
δu	3.89×10^{-4}	n/a	in.
δv	3.89×10^{-4}	n/a	in.

[a]based on 40 calibration points

RESULTS

In final form, ready for use in passive range estimation research, the data base contains time-correlated measurements of

1. imagery data
2. sensor velocity and angular rates, in sensor coordinates
3. sensor internal calibration parameters
4. sensor external calibration parameters
5. sensor position and orientation, in Earth coordinates
6. obstacle locations, in Earth coordinates

The first three data elements are required for performing passive range estimation. The fourth element allows range estimates in sensor coordinates to be expressed in terms of the rotorcraft body frame so that obstacle information can be displayed to the pilot or used by the flight control system. The final two data elements are used to validate the range estimates obtained from a passive range estimation algorithm. Additionally, since the sensor position and orientation histories are known, a global model can be developed that includes all obstacles encountered by the rotorcraft throughout its flight.

Figure 7 shows one image collected during a flight test, with the associated sensor states and true-range data. In the flight-test scenario depicted, several vehicles were stationed along a runway ramp to serve as obstacles around which the rotorcraft maneuvered. Apparent in the image are the time stamp and several features, each of whose true range has been measured. The sensor calibration parameters (which are time invariant) are those given in table 2.

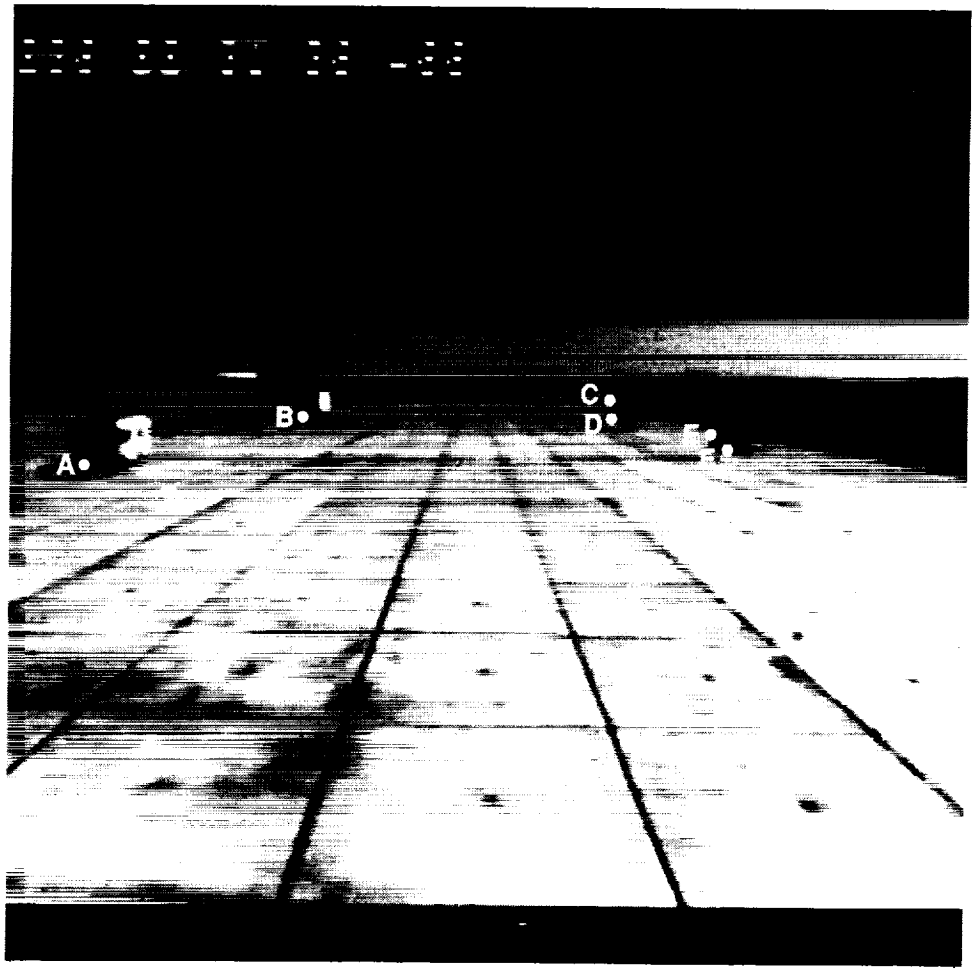

$$V_s = [0.6, -1.8, 38.6]^T \text{ ft/sec}$$

$$\omega_s = [-0.19, -0.39, 0.44]^T \text{ deg/sec}$$

Object	ρ_{x_s} (ft)	ρ_{y_s} (ft)	ρ_{z_s} (ft)
A	–66	1	184
B	–65	–15	435
C	69	–31	580
D	68	–19	561
E	69	–8	334
F	69	–3	312

Figure 7. Sample data from a flight test.

CONCLUDING REMARKS

A complete "real world" data base has been developed from data acquired through rotorcraft test flight, to enable further research into the use of passive range estimation for obstacle avoidance during NOE flight. The data base has been designed to incorporate measurements required by a wide variety of single-sensor, passive range estimation algorithms, so as to serve as a benchmark for comparison of different methods. During the data preparation, a camera calibration methodology was developed to obtain accurate knowledge of the sensor's characteristic parameters. The camera calibration technique as well as the data base can potentially be applied to research in robotics and the autonomous navigation of vehicles.

Future directions include a comparative study, based on the data set described here, of current passive range estimation algorithms followed by further research on the most promising algorithms. There is also interest in applying the experience gained in developing the single-camera data base to the production of a similar data base to support research in multicamera (stereoscopic) methods of passive range estimation.

To obtain the images in digitized form, along with the sensor states, sensor calibration parameters, and true range measurements, researchers in passive range estimation may contact the author.

REFERENCES

1. Cheng, V. H. L.; and Sridhar, B.: Considerations for Automated Nap-of-the-Earth Rotorcraft Flight. American Control Conference, Atlanta, GA, June 15-17, 1988.

2. Ballard, D. H.; and Brown, C. M.: Computer Vision. Prentice-Hall, 1982.

3. Sridhar, B.; and Phatak, A. V.: Simulation and Analysis of Image-Based Navigation System for Rotorcraft Low-Altitude Flight. Amer. Helicopter Soc. Meeting on Automation Applications of Rotorcraft, Atlanta, GA, Apr. 4-6, 1988.

4. Sridhar, B.; Cheng, V. H. L.; and Phatak, A. V.: Kalman Filter Based Range Estimation for Autonomous Navigation Using Imaging Sensors. 11th IFAC Symposium on Automatic Control in Aerospace, Tsukuba, Japan, July 1989.

5. Menon, P. K. A.; and Sridhar, B.: Passive Navigation Using Image Irradiance Tracking. AIAA Guidance, Navigation, and Control Conference, Boston, MA, Aug. 1989.

6. Bhanu, B.; Roberts, B.; and Duncan, D.: Obstacle Detection During Rotorcraft Flight. First Annual Report for National Aeronautics and Space Administration. Contract no. NAS2-12800, Honeywell Systems and Research Center, Apr. 1989.

7. Tsai, R. Y.: A Versatile Camera Calibration Technique for High-Accuracy 3D Machine Vision Metrology Using Off-the-Shelf TV Cameras and Lenses. IEEE Journal of Robotics and Automation, vol. RA-3, no. 4, Aug. 1987, pp. 323-344.

NASA
National Aeronautics and Space Administration

Report Documentation Page

1. Report No.	2. Government Accession No.	3. Recipient's Catalog No.
NASA TM-102809		

4. Title and Subtitle	5. Report Date
Flight Data Acquisition Methodology for Validation of Passive Ranging Algorithms for Obstacle Avoidance	October 1990
	6. Performing Organization Code
7. Author(s)	8. Performing Organization Report No.
Phillip N. Smith	A-90124
	10. Work Unit No.
	505-66-51
9. Performing Organization Name and Address	11. Contract or Grant No.
Ames Research Center Moffett Field, CA 94035-1000	
	13. Type of Report and Period Covered
12. Sponsoring Agency Name and Address	Technical Memorandum
National Aeronautics and Space Administration Washington, DC 20546-0001	14. Sponsoring Agency Code

15. Supplementary Notes

Point of Contact: Phillip N. Smith, Ames Research Center, MS 210-9, Moffett Field, CA 94035-1000 (415) 604-5469 or FTS 464-5469

The information in this paper was presented at the 46th Annual Forum and Technology Display of the American Helicopter Society, Washington, DC, May 21-23, 1990.

16. Abstract

The automation of low-altitude rotorcraft flight depends on the ability to detect, locate, and navigate around obstacles lying in the rotorcraft's intended flightpath. Computer vision techniques provide a passive method of obstacle detection and range estimation, for obstacle avoidance. Several algorithms based on computer vision methods have been developed for this purpose using laboratory data; however, further development and validation of candidate algorithms require data collected from rotorcraft flight. A data base containing low-altitude imagery augmented with the rotorcraft and sensor parameters required for passive range estimation is not readily available. This paper focuses on the methodology used to develop such a data base from flight-test data consisting of imagery, rotorcraft and sensor parameters, and ground-truth range measurements. As part of the data preparation, a technique for obtaining the sensor calibration parameters is described. The data base will enable the further development of algorithms for computer vision-based obstacle detection and passive range estimation, as well as provide a benchmark for verification of range estimates against ground-truth measurements.

17. Key Words (Suggested by Author(s))	18. Distribution Statement
Computer vision Passive range estimation Helicopter test flight Camera calibration	Unclassified-Unlimited Subject Category - 04

19. Security Classif. (of this report)	20. Security Classif. (of this page)	21. No. of Pages	22. Price
Unclassified	Unclassified	16	A02

For sale by the National Technical Information Service, Springfield, Virginia 22161